# Direct Measurement of Spindle Motion Error Using a Regular Crystalline Lattice and a Scanning Tunneling Microscope

**Patamaporn Chaikool[1], Masato Aketagawa[1,#] and Eiki Okuyama[2]**

1 Department of Mechanical Engineering, Nagaoka University of Technology, Nagaoka, Niigata 940-2188 Japan
2 Department of Mechanical Engineering, Akita University, Akita 010-8502 Japan
# Corresponding Author / E-mail: masatoaa@vos.nagaokaut.ac.jp,TEL: +81-258-47-9741, FAX: +81-258-47-9770

KEYWORDS: Spindle motion error, Regular crystalline lattice, Scanning tunneling microscope, Picometer

*Metrology tools with the ability to measure spindle motion error on the order of a nanometer are required due to recent advances in nanotechnology. We propose a direct measurement method for the radial motion error of a precision spindle using a regular crystalline lattice and a scanning tunneling microscope (STM). A highly oriented pyrolytic graphite (HOPG) crystal combined with an STM is used as a two-dimensional reference scale. The measurement principle and the preliminary experimental results are discussed in this article. The preliminary experimental results demonstrated that the proposed method has the capability to incorporate a two-dimensional encoder to measure the spindle motion error.*

Manuscript received: January 18, 2008 / Accepted: June 9, 2008

## NOMENCLATURE

$\boldsymbol{a}_i$ = unit lattice vector ($i$ = 1, 2)
$\boldsymbol{d}(\theta)$ = radial motion error
$\boldsymbol{k}_i$ = reciprocal vector ($i$ = 1, 2)
$m(\theta)$ = number of lattice spaces in the $\boldsymbol{a}_1$ direction
$n(\theta)$ = number of lattice spaces in the $\boldsymbol{a}_2$ direction
$R(\theta)$ = rotation matrix
$\boldsymbol{r}$ = lateral displacement vector
$Z(\boldsymbol{r})$ = topographical height of the HOPG crystal
$\delta_{ij}$ = Kronecker delta
$\theta$ = rotation angle

## 1. Introduction

With recent advances in nanotechnology and ultra-precision engineering, industrial metrology requires a reduction in the spindle rotation error to the nanometer or sub-nanometer level.[1-3] Spindle measurements by conventional methods will have contributions from the spindle motion error and the form error of the target artifact. Therefore, methods for separating the spindle motion error from the artifact error are necessary.[4,5] However, the ability of conventional spindle measurements to achieve nanometer- or sub-nanometer-level accuracy is questionable.

When crystals are stress-free in a regular crystalline lattice, the lattice spacing is approximately 0.2 to 0.3 nm and is uniform and stable over a long range. A scanning tunneling microscope (STM)[6] is capable of observing the atomic image of a crystalline surface. Previously, we proposed a two-dimensional (2-D) displacement encoder with 10-pm resolution that uses a highly oriented pyrolytic graphite (HOPG) crystal and a multi-tunneling-probe STM (MTP-STM).[7]

In this research, a HOPG crystal placed on top of a spindle and used as a 2-D reference scale is observed with an MTP-STM. A high-speed lateral dither modulation is applied to the tip scanner to accommodate the MTP-STM technique. A direct measurement technique based on two unit lattice vectors from the crystalline lattice is used to determine the spindle motion error. The spindle motion error can be measured directly with 10-pm resolution without using a separation method. A comparison of the proposed method with conventional spindle measurements will be performed in the future. The measurement principle and preliminary experimental results are discussed in this article.

## 2. Measurement Principle

The principle for direct measurements of the spindle motion error based on a 2-D encoder and a microscope is illustrated in Figure 1. The measurement principle can be described as follows:

1) A 2-D reference scale is set on top of the spindle of interest, and a microscope is laterally fixed and mounted over the scale, as shown in Figure 1(a).
2) When the spindle rotates, the microscope observes the combined lateral (radial) motion and spindle rotational motion.
3) If the microscope rotates simultaneously with the spindle but maintains its lateral position, the radial motion of the spindle can be measured.
4) If the microscope and the 2-D scale are replaced by an STM and an HOPG crystal, as shown in Figure 1(b), radial motion

measurements with 10-pm resolution are possible.

Previous research[8] showed that a microscope could be used for the spindle error measurement; however, the microscope did not rotate.

Figure 2 shows our proposed system for measuring the radial spindle motion error by combining an STM and an HOPG crystal. The measurement system consists of a fixed *XYZ* tip scanner, an STM tip, an ultra-precise spindle, the HOPG crystal, a rotary encoder, an STM controller, a digital signal processor (DSP) with A/D and D/A converters, a piezoelectric (PZT) amplifier, a reference cylinder, and capacitive displacement sensors. In the system, the HOPG is used as a 2-D reference scale and installed on the top-center surface of the spindle of interest. The fixed STM tip scanner and the dithered STM tip are set on the HOPG crystal. A high-speed lateral-circular dither modulation is applied to the *XY* scanner such that the STM tip is positioned at the appropriate points on the HOPG crystalline surface in semi-real time. These points rotate with the spindle.

When the spindle rotates, a relative 2-D lateral displacement between the STM scanner and the top surface of the spindle can be determined from the multi-current signals of the points. Using the multi-current signals, the 2-D lateral displacement of the top surface of the spindle can be calculated from a linear sum of the two unit-lattice vectors $\boldsymbol{a}_1$ and $\boldsymbol{a}_2$ of the HOPG crystalline surface. The lattice spacing of $|\boldsymbol{a}_1|$ or $|\boldsymbol{a}_2|$ on the HOPG crystal[9] is 0.246 nm, and the intersecting angle between $\boldsymbol{a}_1$ and $\boldsymbol{a}_2$ is 60°. A displacement interpolation that is less than the HOPG lattice spacing of 0.246 nm can also be performed. Capacitive displacement sensors are installed to compare the proposed method with conventional methods, including reversal,[10,11] multi-step,[12,13] and multi-probe[14,15] techniques.

To achieve a lateral-circular dither motion, two sinusoidal signals with a 90° phase difference and the desired amplitudes are applied to the *XY* tip scanner. Figure 3 shows an ideal surface structure of the HOPG crystal. The tip moves circularly along the specific points from A to F on the crystalline surface, as shown in Figure 3. The tunneling currents at points A to F are obtained in semi-real time.

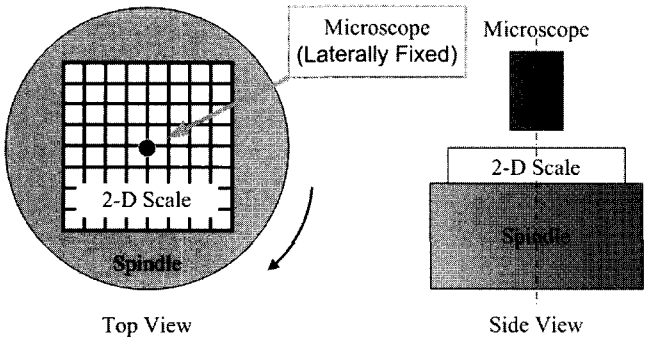


(a) Measurement system using the microscope and a 2-D scale

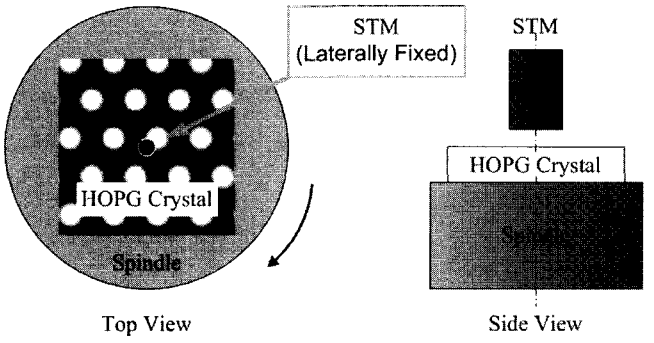


(b) Measurement system using an STM and an HOPG crystal as a reference scale

Fig. 1 Measurement system for the spindle motion error

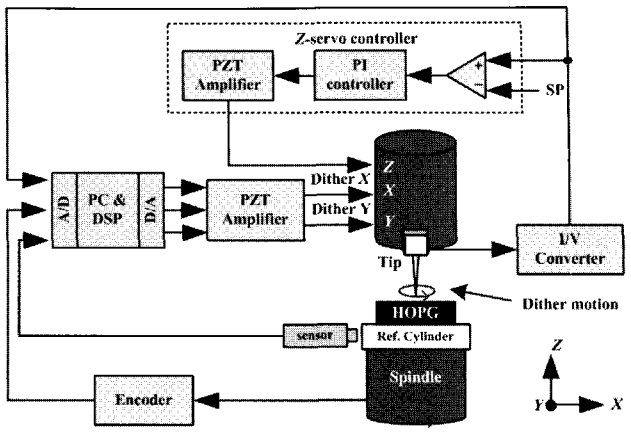


Fig. 2 Spindle motion error measurement system

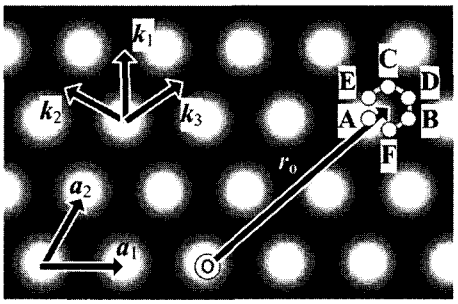


Fig. 3 Ideal surface structure of the HOPG crystal and the specific points for the MTP-STM method ( $\overline{AB} = \frac{1}{2}\boldsymbol{a}_1$ and $\overline{AC} = \frac{1}{2}\boldsymbol{a}_2$ )

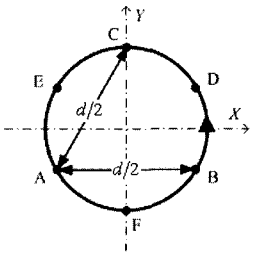


Fig. 4 Trajectory of high-speed lateral dither modulation applied to the STM tip

We assume that the coordinate system on the top surface of the spindle (the HOPG surface) is *o-xyz*, and the fixed coordinate system outside the spindle is *o'-x'y'z'*. The relationship between the lateral vectors $\boldsymbol{r}' = (x', y')$ and $\boldsymbol{r} = (x, y)$ in the *o'-x'y'z'* and *o-xyz* systems, respectively, is

$$\boldsymbol{r}' = R(\theta)\boldsymbol{r} + \boldsymbol{d}(\theta) \text{ or } \boldsymbol{r} = R(-\theta)\{\boldsymbol{r}' - \boldsymbol{d}(\theta)\}, \quad (1)$$

where $\boldsymbol{d}(\theta)$ is the lateral displacement vector of the rotating center (a radial motion error) and $R(\theta)$ is the rotation matrix. The *o-xyz* system rotates with $R(\theta)$ against the *o'-x'y'z'* system. Vector $\boldsymbol{r}'_{od}$ of the center of the dither motion is the assumed point of origin of the *o'-x'y'z'* system. When the center of the dither motion is locked ($\boldsymbol{r}'_{od} = 0$), vector $\boldsymbol{r}_{od}$ of the *o-xyz* system is given by

$$\boldsymbol{r}_{od} = R(-\theta)\{\boldsymbol{r}'_{od} - \boldsymbol{d}(\theta)\} = -R(-\theta)\boldsymbol{d}(\theta), \quad (2)$$

where $\boldsymbol{r}_{od}$ is the linear sum of unit vectors $\boldsymbol{a}_1$ and $\boldsymbol{a}_2$ on the HOPG crystalline surface. Therefore, $\boldsymbol{r}_{od}$ can be represented by

$$\boldsymbol{r}_{od} = m(\theta)\boldsymbol{a}_1 + n(\theta)\boldsymbol{a}_2 . \quad (3)$$

Then,

$$\boldsymbol{d}(\theta) = -R(\theta)\{m(\theta)\boldsymbol{a}_1 + n(\theta)\boldsymbol{a}_2\} . \quad (4)$$

Equation (4) shows that it is possible to determine the lateral displacement vector (the radial motion error) $\boldsymbol{d}(\theta)$ if $m(\theta)$ and $n(\theta)$ can be determined.

To determine $m(\theta)$ and $n(\theta)$, a high-speed lateral dither modulation is applied to the STM tip to collect the tunneling current signals from points A to F, as shown in Figure 4. The lateral displacement vectors at points A' to F' in the *o'-x'y'z'* system are given by

$$\boldsymbol{r}'_A = R(\theta)\left(-\tfrac{1}{6}\boldsymbol{a}_1 - \tfrac{1}{6}\boldsymbol{a}_2\right) , \quad (5a)$$

$$\boldsymbol{r}'_B = R(\theta)\left(\tfrac{1}{3}\boldsymbol{a}_1 - \tfrac{1}{6}\boldsymbol{a}_2\right) , \quad (5b)$$

$$\boldsymbol{r}'_C = R(\theta)\left(-\tfrac{1}{6}\boldsymbol{a}_1 + \tfrac{1}{3}\boldsymbol{a}_2\right) , \quad (5c)$$

$$\boldsymbol{r}'_D = R(\theta)\left(\tfrac{1}{6}\boldsymbol{a}_1 + \tfrac{1}{6}\boldsymbol{a}_2\right) , \quad (5d)$$

$$\boldsymbol{r}'_E = R(\theta)\left(-\tfrac{1}{3}\boldsymbol{a}_1 + \tfrac{1}{6}\boldsymbol{a}_2\right) , \quad (5e)$$

$$\boldsymbol{r}'_F = R(\theta)\left(\tfrac{1}{6}\boldsymbol{a}_1 - \tfrac{1}{3}\boldsymbol{a}_2\right) . \quad (5f)$$

From Equation (5), points A' to F' rotate simultaneously along the spindle axis. From Equations (1) to (5), the lateral displacement vectors in the *o-xyz* system at points A to F are

$$\boldsymbol{r}_A = \left\{m(\theta) - \tfrac{1}{6}\right\}\boldsymbol{a}_1 + \left\{n(\theta) - \tfrac{1}{6}\right\}\boldsymbol{a}_2 , \quad (6a)$$

$$\boldsymbol{r}_B = \left\{m(\theta) + \tfrac{1}{3}\right\}\boldsymbol{a}_1 + \left\{n(\theta) - \tfrac{1}{6}\right\}\boldsymbol{a}_2 , \quad (6b)$$

$$\boldsymbol{r}_C = \left\{m(\theta) - \tfrac{1}{6}\right\}\boldsymbol{a}_1 + \left\{n(\theta) + \tfrac{1}{3}\right\}\boldsymbol{a}_2 , \quad (6c)$$

$$\boldsymbol{r}_D = \left\{m(\theta) + \tfrac{1}{6}\right\}\boldsymbol{a}_1 + \left\{n(\theta) + \tfrac{1}{6}\right\}\boldsymbol{a}_2 , \quad (6d)$$

$$\boldsymbol{r}_E = \left\{m(\theta) - \tfrac{1}{3}\right\}\boldsymbol{a}_1 + \left\{n(\theta) + \tfrac{1}{6}\right\}\boldsymbol{a}_2 , \quad (6e)$$

$$\boldsymbol{r}_F = \left\{m(\theta) + \tfrac{1}{6}\right\}\boldsymbol{a}_1 + \left\{n(\theta) - \tfrac{1}{3}\right\}\boldsymbol{a}_2 . \quad (6f)$$

The topographical height $Z(r)$ of the HOPG crystal can be represented approximately by

$$Z(\boldsymbol{r}) = \sum_{i=1}^{3} A_i \cos(2\pi \boldsymbol{k}_i \cdot \boldsymbol{r}) , \quad (7)$$

where $\boldsymbol{r}$ is the lateral displacement vector and $\boldsymbol{k}_i$ is the reciprocal vector. The relationship between the reciprocal vector $\boldsymbol{k}_i$ and the unit lattice vector $\boldsymbol{a}_i$ is

$$\boldsymbol{a}_i \cdot \boldsymbol{k}_j = \delta_{ij} , \quad (8)$$

$$\boldsymbol{k}_3 = \boldsymbol{k}_1 - \boldsymbol{k}_2 , \quad (9)$$

where $\delta_{ij}$ is the Kronecker delta. From Equations (6) to (9),

$$Z(\boldsymbol{r}_A) + Z(\boldsymbol{r}_B) = 2A_2 \cos\left\{2\pi\left(n(\theta) - \tfrac{1}{6}\right)\right\} , \quad (10a)$$

$$Z(\boldsymbol{r}_D) + Z(\boldsymbol{r}_E) = 2A_2 \cos\left\{2\pi\left(n(\theta) + \tfrac{1}{6}\right)\right\} , \quad (10b)$$

$$Z(\boldsymbol{r}_A) + Z(\boldsymbol{r}_C) = 2A_1 \cos\left\{2\pi\left(m(\theta) - \tfrac{1}{6}\right)\right\} , \quad (10c)$$

$$Z(\boldsymbol{r}_D) + Z(\boldsymbol{r}_F) = 2A_1 \cos\left\{2\pi\left(m(\theta) + \tfrac{1}{6}\right)\right\} . \quad (10d)$$

This leads to

$$\left[Z(\boldsymbol{r}_A) + Z(\boldsymbol{r}_B)\right] + \left[Z(\boldsymbol{r}_D) + Z(\boldsymbol{r}_E)\right] = 2A_2 \cos 2\pi n(\theta), \quad (11a)$$

$$\left[Z(\boldsymbol{r}_A) + Z(\boldsymbol{r}_B)\right] - \left[Z(\boldsymbol{r}_D) + Z(\boldsymbol{r}_E)\right] = 2\sqrt{3}A_2 \sin 2\pi n(\theta), \quad (11b)$$

$$\left[Z(\boldsymbol{r}_A) + Z(\boldsymbol{r}_C)\right] + \left[Z(\boldsymbol{r}_D) + Z(\boldsymbol{r}_F)\right] = 2A_1 \cos 2\pi m(\theta), \quad (11c)$$

$$\left[Z(\boldsymbol{r}_A) + Z(\boldsymbol{r}_C)\right] - \left[Z(\boldsymbol{r}_D) + Z(\boldsymbol{r}_F)\right] = 2\sqrt{3}A_1 \sin 2\pi m(\theta). \quad (11d)$$

$Z(\boldsymbol{r}_A) - Z(\boldsymbol{r}_F)$ can be determined from the tunneling currents at points A to F, and $m(\theta)$ and $n(\theta)$ can be determined from the integers and fractions given by $(\cos 2\pi m(\theta), \sin 2\pi m(\theta))$ and $(\cos 2\pi n(\theta), \sin 2\pi n(\theta))$ in Equation (11). The lateral displacement vector $\boldsymbol{d}(\theta)$ can be represented formally by

$$\boldsymbol{d}(\theta) = -R(\theta)\left\{\begin{array}{l}\left[\frac{1}{2\pi}\tan^{-1}\left(\frac{1}{\sqrt{3}}\left(\frac{z(\boldsymbol{r}_A)+z(\boldsymbol{r}_C)-z(\boldsymbol{r}_D)-z(\boldsymbol{r}_F)}{z(\boldsymbol{r}_A)+z(\boldsymbol{r}_C)+z(\boldsymbol{r}_D)+z(\boldsymbol{r}_F)}\right)\right)\right]\boldsymbol{a}_1 \\ +\left[\frac{1}{2\pi}\tan^{-1}\left(\frac{1}{\sqrt{3}}\left(\frac{z(\boldsymbol{r}_A)+z(\boldsymbol{r}_B)-z(\boldsymbol{r}_D)-z(\boldsymbol{r}_E)}{z(\boldsymbol{r}_A)+z(\boldsymbol{r}_B)+z(\boldsymbol{r}_D)+z(\boldsymbol{r}_E)}\right)\right)\right]\boldsymbol{a}_2\end{array}\right\} \quad (12)$$

Using this technique, the lateral displacement vector $\boldsymbol{d}(\theta)$ can be measured using the tunneling currents at points A to F (A' to F'). This method is known as the six-point method.

The measurement procedure for the spindle motion error can be summarized as follows.

1) To determine the crystalline orientations of the HOPG crystal at the initial axial position, fix the spindle and observe the HOPG surface with an STM. Next, determine the amplitude of the lateral-circular dither modulation and collect data points for points A to F shown in Figure 4.
2) Apply the lateral-circular dither modulation to the STM tip. Rotate the spindle and measure the rotation angle $\theta$ with the rotary encoder. Collect the tunneling current signals from points A to F (A' to F'), calculate the values of Equations (10) to (12), and then determine $m(\theta)$ and $n(\theta)$. Determine the radial motion error $\boldsymbol{d}(\theta)$ with Equation (4) or (12).
3) Rotate to the next angle $\theta + \Delta\theta$, where $\Delta\theta$ is the measurement sampling angle interval (or the rotary encoder resolution), and repeat step 2.
4) Integrate $\boldsymbol{d}(\theta)$ over one or more revolutions.

The measurement sampling angle interval $\Delta\theta$ depends on the average distance $L$ between the spindle rotation center and the STM tip. Due to the sampling theory, in order to obtain continuous atomic signals with the STM tip, the condition $L\Delta\theta \le 0.5|\boldsymbol{a}_i|$, where $|\boldsymbol{a}_i|$ is the lattice spacing, must be satisfied. To attain good atomic signals, the condition $L\Delta\theta \le 0.1|\boldsymbol{a}_i|$ is preferable. If we assume $L$ = 0.5 μm, which is not difficult to achieve, then $\Delta\theta = 5\times10^{-5}$ rad. The measurement speed of the proposed method is approximately 100 nm/s.[4]

## 3. Preliminary Experimental Results Obtained Using the Six-Point Method

Although the spindle motion error measurement system is still under construction, the ability to measure displacement using the six-point method is possible and is examined in this section. Figure 5 shows the preliminary experimental system. The system contains an STM tip with an *XYZ* tip scanner, a sample *XY* stage on which the HOPG crystal is set, a *Z* servo controller with an I/V converter, PC and DSP controllers with A/D and D/A controllers, and a PZT amplifier. In the experiment, a lateral-circular dither motion was applied to the *XY* tip scanner to implement the six-point method. Simultaneously, tunneling current signals corresponding to the six A to F points were collected with an A/D converter. A raster scan signal

was applied to the sample $XY$ stage, and atomic STM images of the A to F points on the HOPG crystal were obtained. The experimental conditions are listed in Table 1.

Figure 6 shows the results of the crystalline orientation separation. Figures 6(a)–(f) contain atomic images of the HOPG crystal based on the tunneling current signals from points A to F, respectively. Figures 6(g) and (h) show the summed images of 6(a) + (b) and 6(a) + (c) given by Equations (10a) and (10c), respectively. Similarly, Figures 6(i) and (j) show the summed images of 6(d) + (e) and 6(d) + (f) given by Equations (10b) and (10d), respectively.

Figures 6(g) and (i) contain the $k_2$ sinusoidal wave signals that were used to determine $n(\theta)$, while $m(\theta)$ can be calculated from the $k_1$ sinusoidal wave signals shown in Figures 6(h) and (j). The cross-sections in Figures 6(g) and (i), and 6(h) and (j) were investigated to determine the phase difference between Equations (10a) and (10b), and between (10c) and (10d), respectively.

Figure 7(a) shows the cross-sectional lines of Figures 6(g), (i), (h), and 6(j). Figure 7(b) shows the difference between Figures 6(g) and (i). Figure 7(c) shows the difference between Figures 6(h) and (j). Figures 7(b) and 7(c) indicate that the phase differences between Figures 6(g) and (i), and between Figures 6(h) and (j) were almost $2\pi/3$ radians, which confirmed the validity of Equation (10). Moreover, it was possible to interpolate $m(\theta)$ and $n(\theta)$ using Equations (10) or (11). This result signified that a 2-D displacement measurement with a resolution of 10% or less of the lattice spacing was possible.

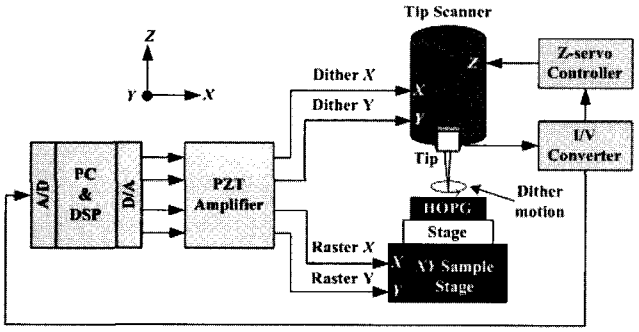


Fig. 5 Preliminary experimental system for the six-point method. To verify the lateral displacement measurement using this method, an $XY$ stage was used instead of a spindle

Table 1 Experimental conditions

| | | |
|---|---|---|
| Scanning conditions | Sample | HOPG |
| | Tip | Pt-Ir / mechanical cut |
| | Bias voltage | 50 mV |
| | Set-point current | 2 nA |
| | Scanned area | 1.8 nm × 1.8 nm (256×256 pixels) |
| | Scan rate | 10.2 Hz / line (25.1 s / image) |
| Dither modulation | Frequency | 5 kHz |
| | Amplitude | ≈ 0.125 nm |

The calculated STM tip displacement from point I to II shown in Figure 6(a) was approximately 2.5 nm. Equation (3) was used, where $m$ = 8 and $n$ = -11.5; $m(\theta)$ and $n(\theta)$ were determined by manual counting.

## 4. Conclusion and Future Work

A new method for measuring the rotation error of an ultra-precision spindle using the MTP-STM method and a regular crystalline lattice was proposed. Using the six-point tunnel current technique, the proposed method can be used to determine the lateral displacement with a resolution of 10 pm. We hypothesize that the proposed method is suitable for directly measuring the spindle motion error. Because the accuracy[16] (or non repetitive run-out motion) of the spindle for a roundness measuring machine (RMM) is ± 5 nm, and such a machine has a low measuring speed of 1 to 20 rpm, we plan to compare the proposed method with conventional spindle measurement techniques using the RMM in the near future.

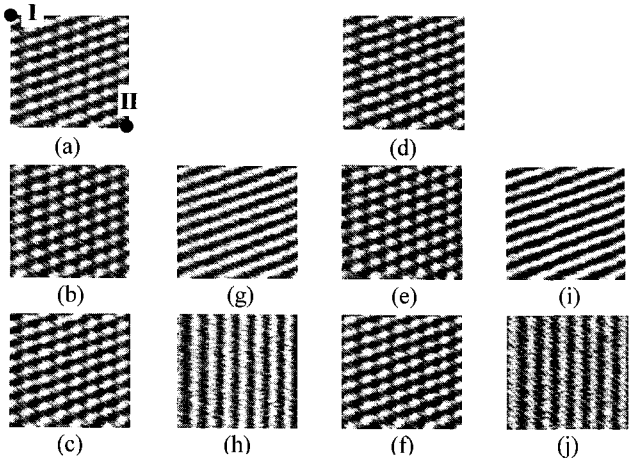


Fig. 6 Separation of the crystalline orientations of the HOPG crystal using the six-point method (g = a + b, h = a + c, i = d + e, j = d + f)

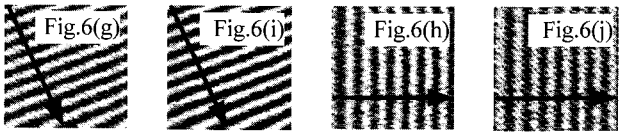


(a) Cross-sectional lines of Figures 6(g), (i), (h), and (j)

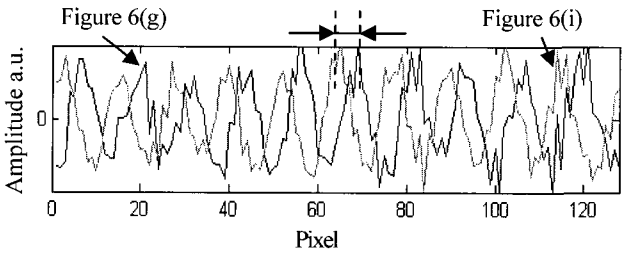


(b) Comparison between Figures 6(g) and (i)

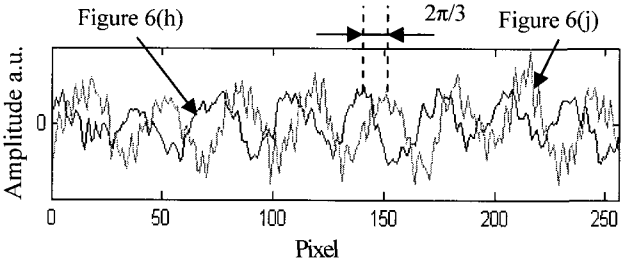


(c) Comparison between Figures 6(h) and (j)

Fig. 7 Cross-section comparison between Figures 6(g), (i), (h), and (j)

## ACKNOWLEDGEMENT

The financial supports of the Research Found of the Japan Society for the Promotion of Science and the Electro-Mechanic Technology Advancing Foundation are gratefully acknowledged.

## REFERENCES

1. Kim, S., "Dynamic analysis on belt-driven spindle system of machine tools," International Journal of Precision Engineering

and Manufacturing, Vol. 3, No. 3, pp. 82-89, 2002.

2. Chernopyatov, Y., Lee, C. and Chung, W., "A new approach increasing the rotational accuracy of ball-bearing spindle by using proper bearing positioning," International Journal of Precision Engineering and Manufacturing, Vol. 4, No. 5, pp. 14-21, 2003.
3. Oiwa, T., "An ultraprecise machining system with a hexapod device to measure six-degree-of-freedom relative motions between the tool and workpiece," International Journal of Precision Engineering and Manufacturing, Vol. 8, No. 2, pp. 3-8, 2007.
4. Marsh, E., Couey, J. and Vallance, R., "Nanometer-Level Comparison of Three Spindle Error Motion Separation Techniques," Journal of Manufacturing Science and Engineering, Vol. 128, No. 1, pp. 180-187, 2006.
5. Okuyama, E., Nosaka, N. and Aoki, J., "Radial Motion Measurement of a High-Revolution Spindle Motor," Measurement, Vol. 40, No. 1, pp. 64-74, 2007.
6. Binnig, G., Rohrer, H., Gerber, Ch. and Weibel, E., "Tunneling through a Controllable Vacuum Gap," Applied Physics Letters, Vol. 40, No. 2, pp. 178-180, 1982.
7. Aketagawa, M., Honda, H., Ishige, M. and Chaikool, P., "Two-Dimensional Encoder with Picometre Resolution using Lattice Spacing on Regular Crystalline Surface as Standard," Measurement Science & Technology, Vol. 18, No. 2, pp. 342-349, 2007.
8. Kyusojin, A. and Sagawa, D., "Development of linear and rotary movement mechanism by using flexible strips," Bulletin of the Japan Society of Precision Engineering, Vol. 22, No. 4, pp. 309-314, 1988.
9. Rerkkumsup, P., Aketagawa, M., Takada, K., Watanabe, T. and Sadakata, S., "Direct Measurement Instrument for Lattice Spacing on Regular Crystalline Surfaces using a Scanning Tunneling Microscope and Laser Interferometry," Review of Scientific Instrument, Vol. 74, No. 1, pp. 1205-1210, 2003.
10. Donaldson, R., "A simple method for separation spindle error from test ball roundness," Annals of CIRP, Vol. 21, No. 1, pp. 125-126, 1972.
11. Horikawa, O., Maruyama, N. and Shimada, M., "A low cost, high accuracy roundness measuring system," Precision Engineering, Vol. 25, No. 3, pp. 200-205, 2001.
12. Evans, C., Hocken, R. and Estler, W., "Self-calibration: reversal, redundancy, error separation, and absolute testing," Annals of CIRP, Vol. 45, No. 2, pp. 617-634, 1996.
13. Estler, W., Evan, C. and Shao, L., "Uncertainty estimation for multi position form error metrology," Precision Engineering, Vol. 21, No. 2-3, pp. 72-82, 1997.
14. Ozono, S., "On a new method of roundness measurement based on the three points method," Proceedings of the 1st International Conference on Production Engineering, pp. 457-462, 1974.
15. Whitehouse, D., "Some theoretical aspects of error separation techniques in surface metrology," Journal of Physics E, Vol. 9, No. 7, pp. 531-536, 1976
16. For example, http://www.taylor-hobson.com/talyrond73.htm.